THE JOURNAL OF PHYSICAL CHEMISTRY B

 VOLUME 107, NUMBER 11, MARCH 20, 2003

ARTICLES

Textural Changes during Topochemical Decomposition of Nanocrystalline $Mg(OH)_2$ to MgO

Maxim S. Mel'gunov,[†,§] Vladimir B. Fenelonov,[†] Elena A. Mel'gunova,[†] Alexander F. Bedilo,[‡] and Kenneth J. Klabunde*[,‡]

Boreskov Institute of Catalysis, Prospekt Akademika Lavrentieva 5, 630090, Novosibirsk, Russian Federation, and Department of Chemistry, Kansas State University, Manhattan, Kansas 66506

Received: June 21, 2002; In Final Form: August 13, 2002

Transformation of nanocrystalline $Mg(OH)_2$ to MgO under dynamic vacuum in a temperature range of 570−770 K was studied by TGA-GCMS, FTIR, HREM, XRD, helium pycnometry, and nitrogen adsorption at 77 K. Several processes are shown to occur during transformation including: (a) release of compounds chemisorbed during preparation of nanocrystalline $Mg(OH)_2$ simultaneously with hydroxide−oxide transformation; (b) fragmentation of nanoparticles at temperatures lower than 670 K; and (c) re-crystallization and sintering of nanoparticles, whose mean size increases and relative number decreases rapidly with temperature above 670 K. A new phenomenon of decrease of the interlayer distance in MgO crystallites with increase of the nanoparticle size was observed.

Introduction

The transformation of $Mg(OH)_2$ prepared from different precursors to the corresponding MgO during thermal treatment was studied extensively in the past (see, e.g., ref 1 and the references within). Conventionally prepared magnesium hydroxide has the structure of hexagonal, smooth crystalline platelets with a size of 10−100 nm. The specific surface area is typically about 10−70 m^2/g and the volume of pores is in the range of 0.1−0.7 cm^3/g. Decomposition at 500−600 K results in pseudomorphous transformation of each single platelet, thus the newly appeared numerous MgO crystals of much smaller size (5−20 nm) form a porous aggregate of the same volume and shape the original platelet had. Thus, porous MgO aggregates appear from nonporous $Mg(OH)_2$ platelets. Increase of a treatment temperature results in sintering of MgO crystals (decrease in their relative number and increase in size). Following the described scenario, one can obtain MgO powder with the specific surface area up to 350 m^2/g.

However, despite a relatively high specific surface area, such conventionally prepared MgO is not efficient in reactions with various hazardous compounds and less than ∼30% of the starting MgO can be involved in the reaction. Thus, special preparation procedures are required to increase the efficiency. One of the ways[2,3] is a process of aerogel preparation (AP-), based on sequential methoxidation of pure Mg metal, hydrolyzation, and supercritical drying, that results in formation of the corresponding hydroxide with some residual methanol and organic solvents (toluene) on the surface. The procedure is followed by vacuum or inert-gas-flow treatment at elevated temperature to convert the hydroxide to oxide as well as to remove organic impurities. Both hydroxide and oxide have high specific surface areas that correspond to very small sizes (3−5 nm) of crystallites, which have been elucidated by XRD and HRTEM observations.[4,5] Because of their very small size in the range of nanometers, these particles are also referred to as *nanoparticles* or *nanocrystals*. It is easy to estimate that a

* Corresponding author. E-mail: kenjk@ksu.ksu.edu.
† Boreskov Institute of Catalysis.
‡ Kansas State University.
§ E-mail: 2max@bk.ru.

10.1021/jp021474i CCC: $25.00
Published on Web 02/22/2003

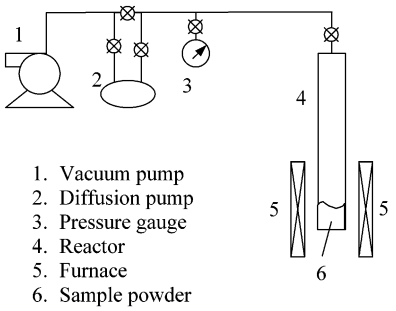

Figure 1. Scheme of the experimental setup for AP-$Mg(OH)_2$ heat treatment.

significant part (up to 40%) of MgO molecules in such nanoparticles are on or close to the surface. The size and shape of these nanoparticles enable them to possess high specific surface reactivity due to high concentrations of edge/corner sites and structural defects on their surface. All these factors play a role in high efficiency of these materials in various heterogeneous reactions, especially reactions with halogenated compounds. For example, nanocrystalline AP-MgO and also AP-CaO and other aerogel prepared oxides were found to be efficient in reactions with organophosphorus compounds such as $(C_2H_5O)_3P{=}O$ or $(C_2H_5O)_3P$ at 500−600 °C,[2,6] halogenated compounds including CCl_4, various Freons, chlorobutenes at 200−500 °C, etc.[7−11] In all these reactions a very large amount of the original oxide (up to 100% depending on particular conditions) is involved in the reaction, resulting in formation of a corresponding solid product (halogenide, phosphate, etc.). This indicates that the reactions proceed not only over the surface of nanoparticles but also have a bulk or *topochemical* character, so transformation of nanoparticles during such reaction should lead to significant textural changes.[11−13]

One of the key factors that should affect MgO reactivity is the texture of the hydroxides that are produced in the aerogel synthesis procedure. Thus, it is crucial to understand the difference between the texture of starting conventionally prepared and AP-hydroxides and changes that take place during dehydration:

$$Mg(OH)_2 \xrightarrow[\text{or hot gas flow}]{\text{above 500 K vacuum}} MgO + H_2O$$

Experimental Section

Sample Preparation. Preparation of starting AP-$Mg(OH)_2$ was described previously.[2−11] In short, clean metal pieces were dissolved in methanol under an inert atmosphere to form metal methoxide, toluene was added, and upon vigorous stirring for a few hours, deionized water was added dropwise to form a hydroxide gel, which was dried of solvent in an autoclave.

The obtained hydroxide was heated under dynamic vacuum (<0.05 Torr) at different temperatures for 24 h to yield partial transformation to the nanometer-sized metal oxide. Further, these samples are referred to as "XXX K", where XXX is the temperature of heat treatment. The scheme of the experimental setup for heat treatment is shown in Figure 1.

The AP-$Mg(OH)_2$ was compared with commercial hydroxide (hereafter referred to as CM-$Mg(OH)_2$) supplied by Alfa Aesar.

Experimental Techniques. Studies of nitrogen adsorption at 77 K were carried out on a NOVA 1200 instrument (Quantachrome). Ultrahigh purity (UHP/Zero) grade nitrogen was supplied by Linweld Corp. The N_2 adsorption isotherms were analyzed by the comparative method[14,15] based on a comparison of the variation of adsorption uptake of experimental

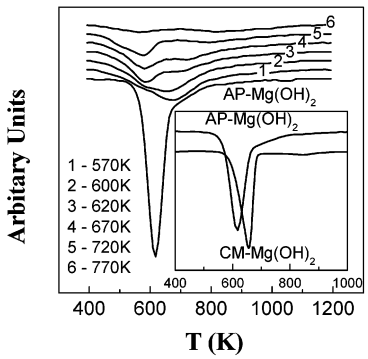

Figure 2. TGA profiles for initial AP-$Mg(OH)_2$ and the samples of AP-$Mg(OH)_2$ heat treated at different temperatures. Temperatures used for heat treatment here and in other figures are 570 K, 600 K, etc. The insert presents TGA profiles for initial AP-$Mg(OH)_2$ and as-received CM-$Mg(OH)_2$.

adsorption isotherm (EI) with a reference adsorption isotherm (RI) for a nonporous sample (generally it is analogous to a more widely used α_S method[16]). The isotherm reported in refs 14 and 15 was used as RI.

IR studies were carried out on a Mattson Research Series 1 FTIR spectrophotometer. IR spectra in a range of 1000−4000 cm^{-1} were measured under dynamic vacuum of $\sim 10^{-5}$ Torr at different temperatures starting from 400 K.

Specific gravity measurements were carried out by helium pycnometry at ambient conditions on an Ultrapycnometer 1000 (Quantachrome) using high purity grade helium supplied by Airgas.

TGA-GCMS studies were carried out on a Shimadzu TGA-50 thermal analyzer coupled to a Shimadzu GC-17 gas chromatograph − mass spectrometer. Studied samples were heated to 1200 K with heating rate of 5 °C/min in UHP grade helium flow of 30 mL/min. In this series of experiments the properties of AP-$Mg(OH)_2$ were compared with those of CM-$Mg(OH)_2$.

XRD studies were carried out on a Scintag-XRD-2000 diffractometer with Cu Kα radiation. Scans were recorded in the 2θ range of 20−80° with scanning rate 5° per minute. Crystallite sizes were calculated from X-ray line broadening using the Scherrer equation.

To minimize possible influence of water vapor, CO_2, etc., adsorption from the air, all the samples were studied immediately after preparation without (N_2 adsorption and He pycnometry) or with minimized (IR, TGA and XRD) contact with air.

Results and Preliminary Analysis of Experimental Data

TGA-GCMS and IR Analysis. TGA profiles for CM-$Mg(OH)_2$ and as-prepared AP-$Mg(OH)_2$ are shown in the insert in Figure 2. One can see well-defined weight loss peaks at 617 K for the AP and at 657 K for the commercial sample. A slight shift of the weight loss maximum to lower temperature for the AP samples in all probability is related to kinetic aspects of decomposition. Another difference between AP- and CM-samples is in the relative mass loss, which is equal to 40.6% for the AP sample and to 30.1% for CM-$Mg(OH)_2$. The weight loss for the commercial sample is very close to the stoichiometric value of 30.8% corresponding to $Mg(OH)_2 \rightarrow MgO$ transformation. The difference between commercial and AP samples is related to the presence of some residual organic solvent in AP-$Mg(OH)_2$. The evidence for this comes from TGA-GCMS profiles of 18 (H_2O), 31 (CH_3OH), and 44 (CO_2) e/z MS signals that are shown in Figure 3a−c, respectively.

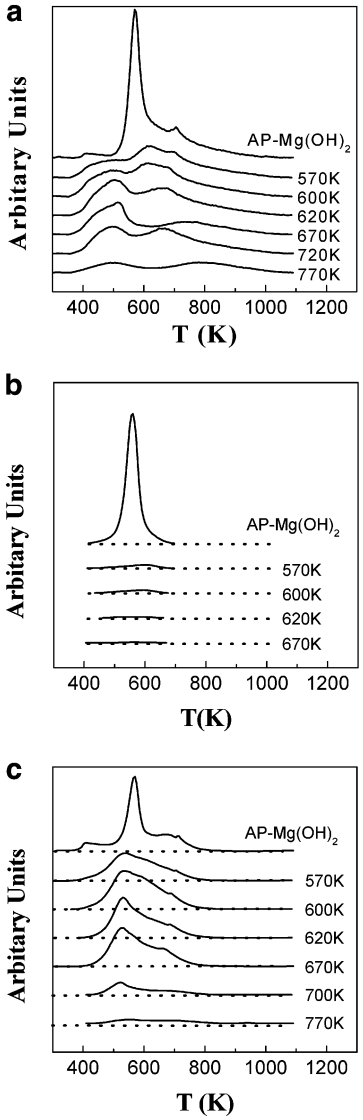

Figure 3. TGA-GCMS profiles of (a) water, (b) methanol, and (c) CO_2 for initial AP-$Mg(OH)_2$ and the samples of AP-$Mg(OH)_2$ heat treated at different temperatures.

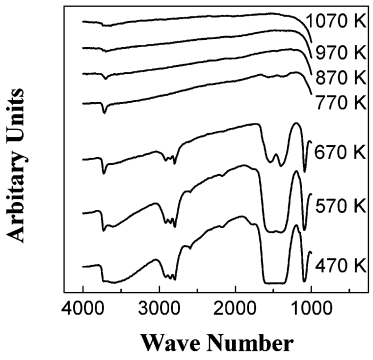

Figure 4. FTIR profiles for 600 K sample subsequently heated in situ at different temperatures.

The maximum of methanol release corresponds to the temperature of 580 K and that of water to 590 K. Simultaneous release of both water and methanol is not surprising because considerable textural and chemical changes occur in this temperature range.

To determine the origin of CO_2, IR studies were carried out for the AP-$Mg(OH)_2$ sample heat-treated at 600 K (Figure 4). In the spectrum of the initial sample one can see strong

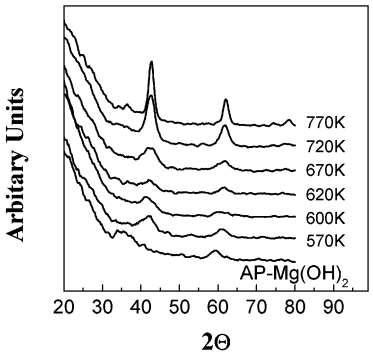

Figure 5. XRD patterns for studied samples.

absorption around 1500 cm^{-1} corresponding to surface carbonates, C−O vibrations of adsorbed methoxide groups at 1080 cm^{-1}, and a complex structure in the C−H region (2800−2950 cm^{-1}), most likely, also associated with the methoxide groups. All these absorption peaks disappear when the temperature in the IR cell is successively increased. No surface carbonate groups were observed at temperatures above 870 K. Based on these results, we conclude that the most probable origin of CO_2 in the TGA-GCMS profiles is related to surface carbonates formed during sample preparation.

Summarizing the results of TGA-GCMS and IR analysis, one can state that as-prepared AP-$Mg(OH)_2$ has an excess of mainly methanol and less CO_2, which are released in the same temperature range as water. No other organic compounds were detected by mass spectrometer in measurable quantities. The amount of methanol in as-prepared AP-$Mg(OH)_2$ can be estimated from the weight loss as 20.5 wt %, water as 16.2 wt %, and CO_2 as 3.8 wt %.

Let us now consider TGA profiles of partially decomposed AP-$Mg(OH)_2$ samples presented in Figure 2. The as-prepared AP-$Mg(OH)_2$ has a sharp peak of weight loss with a maximum at 617 K. Successive heat pretreatment results in decrease of the original peak intensity while a second weight loss peak appears in the temperature range of 650−900 K. The low temperature peak mainly corresponds to water release, as it follows from the TGA-GCMS profiles for H_2O, CH_3OH, and CO_2 presented in Figure 3. Water release profiles in the low-temperature range look very similar to the TGA profiles. On the other hand, the amounts of CO_2 released from samples according to the TGA-GCMS profiles remain very low for heat-treated samples, indicating that very little coke or carbonates are formed during heat pretreatment. IR spectra presented in Figure 4 allowed us to establish the nature of released water. Two absorption peaks at 3600 cm^{-1} corresponding to associated OH groups and at 3720 cm^{-1} corresponding to isolated surface OH groups are observed. Successive in situ thermal treatment results in elimination of both peaks. Associated water comes out first at temperatures less than 700 K, while isolated OH groups remain until 970 K. The values of released water, methanol, and CO_2 weights calculated per weights of starting materials are summarized in Table 1.

Weakly bound H_2O that is released during the TGA experiments at temperatures lower than the temperature of preliminary heat treatment is worthy of separate discussion. It can be explained by the possibility of sample contact with ambient water vapor despite preparation of samples for TGA analysis in a drybox filled with 99.95% pure argon. The TGA pan with the sample was exposed to ambient air for several seconds in order to place it into TGA setup and some water vapor adsorption may have taken place. Further on we shall consider

TABLE 1: TGA Analysis of Studied Samples

sample	AP-$Mg(OH)_2$ as-prepared	treatment temperature, K					
		570	600	620	670	720	770
$Y = m_{ox}/m_{\Sigma}$ as derived from TGA	0.594	0.79	0.779	0.795	0.813	0.859	0.914
Compounds Released during TGA Analysis, g/g $_{composite}$							
H_2O	0.162	0.148	0.164	0.172	0.150	0.130	0.078
Released at low temperatures (associated)		0.046	0.074	0.091	0.095	0.095	0.048
Released at high temperatures (isolated)		0.102	0.090	0.081	0.055	0.035	0.030
CH_3OH	0.205	0.018	0.015	0.006	0.002	n/d	n/d
CO_2	0.038	0.036	0.046	0.039	0.042	0.013	0.008
Relative weight of impurities including water released at low temperatures	0.243	0.100	0.135	0.136	0.139	0.108	0.056

TABLE 2: Textural Characteristics of Solid Phase during $Mg(OH)_2 \rightarrow MgO$ Transformation

sample	AP-$Mg(OH)_2$ as-prepared	treatment temperature, K					
		570	600	620	670	720	770
BET surface area, m^2/g							
A_{BET}	641	697	655	648	652	475	412
C_{BET}	81	82	71	52	64	64	68
Comparative surface area A, m^2/g	765	859	791	782	787	593	468
Ordinate axis intercept on comparative plot, cm^3/g	−0.07	−0.07	−0.06	−0.07	−0.06	−0.05	−0.03
Specific density, ρ, g/cm^3	1.77	2.52	2.44	3.05	2.79	3.18	3.12
Average size of nanoparticles, *d*, nm							
Adsorption							
BET method	5.3	3.4	3.8	3.0	3.3	4.0	4.7
Comparative method	4.4	2.8	3.1	2.5	2.7	3.2	4.1
XRD							
200 reflex	2.1 (101 plane)	2.5	3.7	3.7	3.6	7.4	12.3
220 reflex	3.1 (102 plane)	5.2	5.3	5.7	6.1	7.4	14.2
Interlayer distance by XRD, nm							
$a = d_{200}$		0.432	0.436	0.432	0.426	0.425	0.423
$a = d_{220}/\sqrt{2}$		0.429	0.429	0.428	0.426	0.424	0.423
Concentration of chemisorbed OH groups over the surface							
Total N_{OH}, groups/nm^2		11.5	13.9	14.8	12.8	14.6	11.1
Low-temperature water		3.4	5.5	6.8	8.0	10.7	7.0
High-temperature water		8.1	8.4	8.0	4.8	3.9	4.1

water released at low temperatures as chemisorbed during contact with air, and the one released at high temperatures as residual after heat treatment. Corresponding quantitative values are presented in Table 1.

XRD Studies. X-ray diffraction patterns are shown in Figure 5. As one can see, the crystalline structure cannot be distinguished well for as-prepared hydroxide. There are only two well-defined reflexes at Bragg's angles 2θ equal to 37 and 59 degrees, which are close to the reference reflexes at $2\theta = 38$ and $2\theta = 58$ for hydroxide with $P2m1$ hexagonal symmetry, correspondingly. Reference hydroxide reflex at $2\theta = 18.5$ could not be seen on the pattern for as-prepared AP-$Mg(OH)_2$ probably due to strong influence of scattering. A rough estimation of AP-$Mg(OH)_2$ crystallite size using the Scherrer equation gives 3.1 nm for reflex at $2\theta = 37$ and 2.1 nm for reflex at $2\theta = 59$. However, poor accuracy in determination of the reflex peak parameters leads to poor accuracy of corresponding size estimation. After heat treatment at 570 K, hydroxide peaks cannot be seen well on the XRD pattern due to low signal/noise ratio. That is why estimation of the degree of hydroxide transformation is impossible from the XRD data. Successive heat treatment at higher temperatures results in an increase of signal/noise ratio, and after 720 K well-defined crystalline MgO structure with $Fm3m$ cubic symmetry is observed. There are two main crystallographic directions for this type of symmetry: [100] with interlayer distance $d_{200} = a$ (a is the structural parameter), and [110] with interlayer distance $d_{220} = a\sqrt{2}$.

The values of mean crystalline size and structural parameter are shown in Table 2. A significant increase in crystalline size is observed after heat treatment at 720 K and higher. It can be concluded that 720 K is the starting point for material sintering and/or re-crystallization. Another distinctive feature observed by X-ray diffraction is a shift of patterns to lower values of 2θ. For example, the 200 reflex is centered at $2\theta = 41.8$, that corresponds to the structural parameter $a = 0.432$ nm. The reference value of a is 0.421 nm for well-crystallized MgO. Calculated values of a for all the samples are shown in Table 2. As one can see, the values of a decrease with the temperature of sample heat treatment and reach 0.423 nm for the sample heat-treated at 770 K. In all possibility this is another factor affecting the efficiency of AP-MgO in various reactions. The increase of interlayer distance between planes of atoms could result in a decrease of molecular interactions in nanoparticles favoring enhanced reactivity of the material.

HREM Studies. A high-resolution electron microscopy image of a 770 K sample is shown in Figure 6. One can see MgO nanoparticles aggregated in a porous 3D network. The average size of nanoparticles is in the range of 2−5 nm. Nanoparticles have cubic form and are interconnected by planes with different shifts. Such interconnection results in the presence of a high concentration of edges on the surface that is definitely one more factor affecting AP-MgO reactivity. It is interesting to note that aggregation of nanoparticles proceeds both in [100] and [110] crystallographic directions, while several neighbor

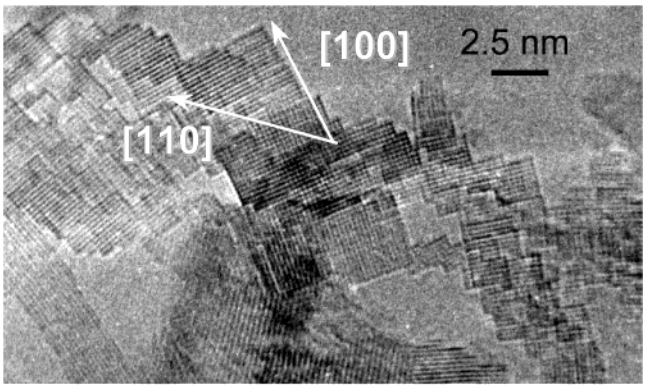

Figure 6. HREM image of 770 K sample, with arrows pointing to assigned crystal faces.

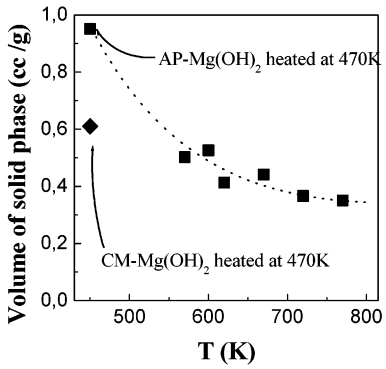

Figure 7. Behavior of solid-phase volume related per weight of MgO.

nanocrystals are united by one lattice. Parallel 100 planes are observed with the best contrast for almost all nanoparticles. The corresponding interplane distance is equal to 0.21 nm that is a half of interlayer distance of 0.423 nm measured by XRD. Parallel planes in [110] direction cannot be observed well, however one can consider [110] direction to be turned to the angle of $\pi/4$ to [100] direction. Aggregation in [100] direction corresponds to joining of nanoparticles by planes and that in [110] direction corresponds to joining by edges and so to shift of neighbor nanoparticles with formation of corresponding surface defects. This result correlates well with the results of nanoparticles size estimation by XRD (see Table 2).

He Pycnometry Studies. The values of specific density, ρ, in g/cc of composite are shown in Table 2. These values were used to calculate the volume of solid phase for convenience related per the weight of MgO using expression (1):

$$v_{\text{solid}} = \frac{1}{\rho Y}, \qquad (1)$$

where $1/Y$ is the ratio of sample mass before and after TGA run (see Table 1). Calculated in such manner, the values of the solid-phase volume are presented in Figure 7. There is a significant deviation between specific volume of solid phase for initial AP-$Mg(OH)_2$ and that for stoichiometric CM-$Mg(OH)_2$. In all probability this deviation can be explained by the presence of chemisorbed methanol and CO_2 in the initial sample. It is easy to estimate the specific volume of these compounds as 0.83 cm^3/g. The corresponding specific densityof chemisorbed compounds will be 1.21 g/cm^3. This value of specific density is 1.5 times higher than the value of 0.79 g/cm^3, which represents the density of liquid (or physically adsorbed) methanol at ambient conditions. This indicates that the condition of methanol and CO_2 in the sample is significantly different from the physically adsorbed state.

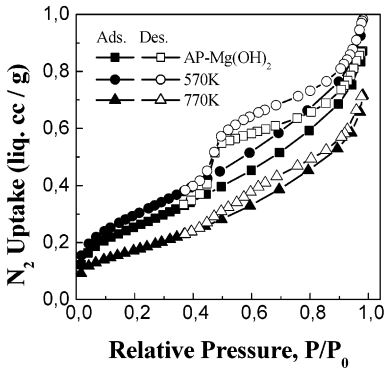

Figure 8. N_2 adsorption/desorption isotherms at 77 K.

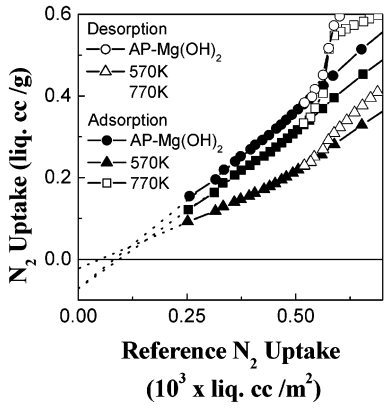

Figure 9. Comparative plots of N_2 adsorption at 77 K.

N_2 Adsorption Studies. N_2 adsorption/desorption isotherms measured at 77 K for initial AP-$Mg(OH)_2$, and samples treated at 570 and 770 K are shown in Figure 8. Isotherms for other samples have the same shape and so are not shown. All the isotherms have capillary-condensation hysteresis loops of the H3 type by IUPAC classification typical for systems containing porous aggregates of primary particles.[16] This texture peculiarity differerentiates AP-$Mg(OH)_2$ porous aggregates from conventionally prepared $Mg(OH)_2$ nonporous platelets.

The values of the specific surface areas, A_{BET}, and the corresponding C_{BET} coefficients determined by BET method (pressure range $0.05 < P/P_0 < 0.3$) are shown in Table 2. Comparative graphs where adsorption branches of isotherms are plotted versus a RI are shown in Figure 9. One can observe a region of linearity on the comparative plots, which corresponds to a region of $0.05 < P/P_0 < 0.4$. The tangent of slope of the interpolation line in the chosen coordinates gives[14,15,17] the surface area, A, of the sample (corresponding values are shown in Table 2).

Interesting features of the observed comparative plots are the negative values of the intercepts on the ordinate axis (see Figure 9 and Table 2). Such negative values are unusual, however not unexpected. Similar negative values were observed for nonporous polar adsorbents modified with molecular dispersed methanol,[14,17] microporous titania modified with *n*-nonane[16] at quantities much lower than mesopore surface monolayer capacity, MCM-41 material modified with octyldimethylsilyl,[18] etc. In all these cases the negativity of the intercepts on the comparative plots corresponds to the surface modification. In refs 14,16,17, shown was the absence of any effect of the intercept negativity on the accuracy of A measurements if the modifier is molecularly dispersed; however, slight deviations can be observed at a high degree of surface coverage with modificator.[18] The successive heat treatment results in aspiring

of the absolute values of comparative intercept to zero and A_{BET} to A that corresponds to "purification" of the surface. This is in good correlation with TGA and FTIR data, which indicate corresponding methanol and CO_2 release. We should note here that the comparative graphs observed in this paper are plotted within the region of relatively high P/P_0 at or above a real monolayer formation. One should expect lack of linearity at comparative plots at very low P/P_0 (see, e.g., ref 19) if the reference adsorbent exhibits surface heterogeneity different from the material under study. However, formation of an adsorbate monolayer results in the decrease of adsorbate−adsorbent interaction and thus the decrease of the corresponding effect, minimizing it at the multilayer region.

Continuing consideration of experimental data, consider that the specific surface area of as-prepared AP-$Mg(OH)_2$ is as high as 765 comparative and 641 m^2/g by the BET method. Thus, taking into account the specific density $\rho = 1.77$ g/cm^3, one can estimate the mean size of AP-$Mg(OH)_2$ nanoparticles using eq 2:

$$d = k_S/k_V \frac{1}{\rho A} \tag{2}$$

with 4.4 nm for comparative A and 5.3 nm for A_{BET} (k_S/k_V—the ratio of surface-size to volume-size form factors—was considered as 6.0 here). Comparing these values to that obtained from XRD we would like to state that the comparative method gives a more reliable value of the surface area than the BET method. After treatment at 570 K−620 K there is a ∼12% increase of specific surface area determined by comparative method and ∼18% increase of A_{BET}, but successive heat treatment results in decreasing of the specific surface area independent of the method of its measuring. The values of the mean nanoparticles size after heat treatment calculated using eq 2 are shown in Table 2.

Discussion

Changes during Decomposition of a Single $Mg(OH)_2$ Nanoparticle. To demonstrate the significance of textural changes that occur in this case, the following estimation of change of a single nanoparticle volume, size, and surface area is presented below. Consider a typical single $Mg(OH)_2$ nanoparticle. Its specific geometrical volume can be derived from the specific density, ρ, of magnesium hydroxide, the reference value of which can be taken as 2.36 g/cm^3. For our purposes the most convenient value to consider is molar volume, υ, of the nanoparticle that can be expressed by eq 3:

$$\upsilon_{Mg(OH)_2} = M/\rho = 24.7 \text{ cm}^3/\text{mol} \tag{3}$$

where $M = 58.3$ g/mol is the molar mass of hydroxide.

Transformation of hydroxide to oxide proceeds without change in the number of Mg ions. So, such a hydroxide nanoparticle being transformed to oxide will have the molar volume υ_{MgO} of 11.3 cm^3/mol (assuming the following to be correct for the oxide: $M = 40.3$ g/mol, $\rho = 3.58$ g/cm^3). As one can see, the ratio of the molar volumes is

$$\nabla = \frac{\upsilon_{MgO}}{\upsilon_{Mg(OH)_2}} = 0.457 \tag{4}$$

This means that the volume of the nanoparticle decreases more than 2-fold. Parameter ∇ is referred to as the Pilling-Bedworth factor.[20] Assuming that the change in shape of this nanoparticle does not significantly affect surface and volume form factors and it did not fragment into several smaller particles, one can also estimate the ratio of its size before and after transformation as $\nabla^{1/3} = 0.77$ and the corresponding ratio of geometrical (not *specific*) surface area for a single particle as $\nabla^{2/3} = 0.593$. This means that size, surface area, and molar volume of the solid phase should decrease significantly during transformation of $Mg(OH)_2$ to MgO. As a result, the small size of AP-$Mg(OH)_2$ nanoparticles and their specific type of aggregation in a porous network can provide some unique characteristics for the material as a whole.

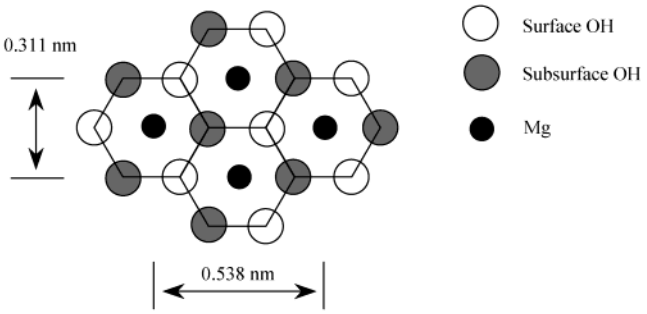

Figure 10. Scheme of a brucite plane from [001] direction.

Characteristics of Original AP-$Mg(OH)_2$. As-prepared AP-$Mg(OH)_2$ was treated at 470 K overnight under vacuum before N_2 adsorption study and after that for 2 h in a flow of ultrapure helium before the TGA-GCMS experiment. Thus, one should expect the amount of physically adsorbed compounds to be negligible. Taking this into account, we assume that the mass balance in as-prepared AP-$Mg(OH)_2$ can be expressed as

$$m = m_{ox} + m_{wat} + m_{met} + m_{car} \tag{5}$$

where m_{ox}, m_{wat}, m_{met}, and m_{car} are the weights of corresponding stoicheometric MgO, H_2O, H_3COH, and CO_2. As it follows from the XRD study, there is no evidence of bulk magnesium methoxide and carbonate phases. Thus, we assume that these compounds are present in the form of surface species over AP-$Mg(OH)_2$. Data in Tables 1 and 2 show that the surface concentration of methanol can be estimated as 5.2 and that of carbonate as 0.7 molecules/nm^2. The scheme of brucite 001 plane surface structure is shown in Figure 10. The main feature of this structure is that the surface Mg layer is interconnected to two OH layers, one at the surface and one in the bulk (subsurface). The ratio of the number of surface OH groups to that of Mg ions is 1.0. The surface concentration of Mg ions in a hexagonal crystal of $P2m1$ symmetry (001 plane) can be estimated as 5.3 ions/nm^2 (similar values can be estimated for other planes). The coincidence between Mg and methoxide and carbonate surface concentrations allows one to consider the surface of as-prepared AP-$Mg(OH)_2$ as being predominantly covered by methoxy and carbonate groups, while OH groups exist only in the bulk of the AP-$Mg(OH)_2$ phase. As the brucite phase is observed in AP-$Mg(OH)_2$, it is possible that methoxy and carbonate groups substitute the corresponding surface OH groups. Due to the absence of surface OH groups in AP-$Mg(OH)_2$, formation of methanol during the TGA experiment appears to proceed according to the following scheme:

$$(H_3CO)^{\uparrow}-Mg_{\square} + Mg_{\square}-(OH)^{\downarrow} \rightarrow H_3COH + MgO_{\square}$$

where $Mg_{\square}$, $(H_3CO)^{\uparrow}-$, and $-(OH)^{\downarrow}$ correspond to a surface Mg framework ion, surface methoxy group, and subsurface

hydroxy group, respectively. Reaction of both surface and subsurface groups explains the simultaneity of methanol and water release during TGA. Methanol cannot be formed before subsurface OH groups start to react. The latter can react only when decomposition of hydroxide to oxide starts.

Textural Changes of Partially Decomposed AP-$Mg(OH)_2$. Formation of a well-defined MgO phase with cubic symmetry accompanied with disappearance of $Mg(OH)_2$ phase, as it follows from the XRD data, is evidence for total transformation of hydroxide nanoparticles to oxide. This process starts at 570 K. The reference temperature range for $Mg(OH)_2$ decomposition is 570−700 K, as follows from the TGA profile for the CM-$Mg(OH)_2$ sample (see Figure 2). According to the TGA profile for as-prepared AP-$Mg(OH)_2$, the temperature range of decomposition shifts to 530−700 K. This shift to a lower temperature range should definitely favor total decomposition. So, a conclusion can be drawn that all hydroxide nanoparticles transform to oxide, while the remaining water is present on the surface mainly as associated and isolated OH groups, as follows from the FTIR data (see Figure 4). One can estimate the number of OH groups over the surface of nanoparticles by eq 6:

$$N_{OH} = N_0 \frac{2\, m_{H_2O}/M_{H_2O}}{A}\ \text{OH groups/m}^2 \qquad (6)$$

where N_0 is the Avogadro number, m_{H_2O} is the weight of released water (see Table 1), A is the surface area of the material; the factor of 2 takes into account that two OH groups form one water molecule. The corresponding values of N_{OH} for total (associated plus isolated) OH groups are brought to Table 2. One can see that the total number as well as the number of associated OH groups per nm^2 remains stable while the number of isolated groups decreases. However, according to the FTIR data, associated OH groups are released with temperature faster than isolated OH groups (Figure 4). In all possibility, this distinction is explained by chemisorption of water from ambient air during the sample transfer to the TGA setup. The active sites, which became free of OH groups during MgO sample preparation, are covered again with new chemisorbed water. An estimate of the theoretically possible number of OH groups per nm^2 taking into account interlayer distance in MgO lattice is ~12.0. One can see that the experimental total number of OH groups is somewhat higher than the theoretical number corresponding to the monolayer of chemisorbed water. To explain this discrepancy, one can assume that some water physisorption takes place during contact of the sample with ambient air. In general, this observation confirms the assumption that nanoparticles are partially covered with chemisorbed OH groups, the surface density of the latter decreasing with growing decomposition temperature. However, even a short contact with ambient air results in recovering of the OH monolayer, followed by much slower physisorption of additional water molecules.

Let us consider a model when *all* nanoparticles are totally transformed and remain covered by a monolayer of chemisorbed water. Assuming all the nanoparticles to be monodispersed the number of nanoparticles, N, in a gram of material can be calculated by eq 7:

$$N = \frac{{k_V}^2}{{k_S}^3} A^3 \rho^2\ \text{nanoparticles/g} \qquad (7)$$

Due to change in mass during decomposition, direct comparison of the number of nanoparticles in 1.0 g of AP-$Mg(OH)_2$ and in 1.0 g of XXX K′ sample is not accurate. To bypass inconvenience aassociated with change in sample mass, it is possible to relate the number of nanoparticles per mole of Mg or mole of MgO, that is equal, because the number of Mg moles does not change during decomposition. To do this, one should multiply N by a factor of $1/YM_{MgO}$. After this manipulation and making an assumption that the effect of change of form factor values is insignificant during transformation, the relative change in the number of nanoparticles is expressed as

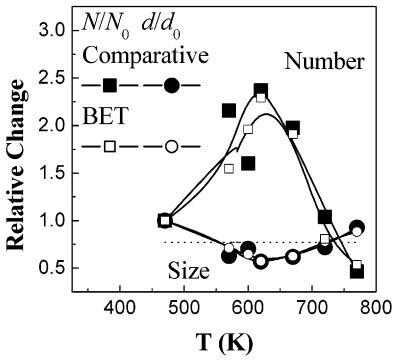

Figure 11. Ratio of nanoparticles number and size to that for as-prepared AP-$Mg(OH)_2$ vs temperature of heat pretreatment.

$$\tilde{N} = \frac{N_{XXX\ K}}{Y_{XXX\ K} M_{MgO}} \frac{Y_{AP-Mg(OH)_2} M_{MgO}}{N_{AP-Mg(OH)_2}} = \left[\frac{A^3\rho^2}{Y}\right]_{XXX\ K} \cdot \left[\frac{Y}{A^3\rho^2}\right]_{AP-Mg(OH)_2} \qquad (8)$$

The values of $\tilde{N}$6 calculated using comparative and BET surface areas are shown in Figure 11. Similar to the definition of $\tilde{N}$, the relative change in the average size of nanoparticles, $\tilde{d}$, can be expressed as

$$\tilde{d} = \frac{d_{XXX\ K}}{d_{AP-Mg(OH)_2}} = \frac{[A\rho]_{AP-Mg(OH)_2}}{[A\rho]_{XXX\ K}} \qquad (9)$$

The corresponding values of $\tilde{d}$ for comparative and BET surface areas are presented in Figure 11. One can observe the coincidence of the values obtained with using the surface areas measured by comparative and BET methods. Thus, even if one of these methods gives inaccurate absolute values of the surface areas, that does not, from our point of view, have an effect on the following very plausible conclusion. Decrease of $\tilde{d}$ is larger than the decrease of 0.77 (dotted line in Figure 11) expected for transformation of a single hydroxide nanoparticle to oxide (see Discussion, first part). Such distinction corresponds to an increase in the number of nanoparticles, probably due to fragmentation[12,13] as well as competitive effect of methanol release and formation of OH monolayer coatings. The maximum relative number of nanoparticles that is about 2.4 times larger than that in as-prepared AP-$Mg(OH)_2$ is achieved after 600 K pretreatment. The mean size of nanoparticles for this point is about 0.58 of that for as-prepared hydroxide. At $T > 620$ K the number of nanoparticles starts to decrease rapidly while their mean size increases. Increase of the nanoparticle size at $T >$ 620 K in all probability is related to sintering of the nanoparticles, the evidence for which is a considerable decrease in the number of nanoparticles (see Figure 11). This indicates that nanoparticle sintering starts at these conditions. Note that this result correlates well with XRD data discussed above.

One can see deviations in the values of nanoparticle size calculated using data from different experimental methods. For example, XRD gives the value of crystalline size of 12.4 nm in the [100] crystallographic direction and 14.3 nm in the [110] crystallographic direction for 770 K sample. Meanwhile, nanoparticle size estimated from HREM and N_2 adsorption data for this sample is ~3 nm and ~4 nm, respectively. This deviation can be easily explained if we consider the HREM image (Figure 6). As one can see, the 770 K sample is formed by interconnected nanocrystals. These nanocrystals are not connected chaotically, but attached to each other in appropriate crystallographic directions. However, probably, due to small size and the large number of nanoparticles, one can expect that the concentration of re-crystallization centers is high. Every such center favors growth of nanocrystallites in random direction. As a result, crystallographic directions of nanocrystallites are isotropically distributed over the sample. So, several nanocrystals form crystallographic ordered domains, and their mean size can be estimated by the size of the corresponding region of coherent diffraction of about 10 nm. In all probability, the same regions of coherent diffraction are observed by XRD. This interesting observation is remarkable and unites the results obtained by different methods.

Conclusion

Summarizing the results of textural consideration, we can conclude that several processes occur during the transformation of AP-$Mg(OH)_2$ to AP-MgO:

(A) Unlike relatively big hexagonal crystalline platelets of conventionally prepared $Mg(OH)_2$, as-prepared nanocrystalline AP-$Mg(OH)_2$ forms porous aggregates of hydroxide nanoparticles covered by residual chemisorbed methanoxy and carbonate groups. Release of chemisorbed compounds during heat treatment proceeds simultaneously with hydroxide−oxide transformation.

(B) Fragmentation of nanoparticles occurs at temperatures lower than 670 K. Fragmentation of such small nanoparticles (size of ~3 nm) during transformation was not expected and indicates that the mean size of oxide phase nuclei is less than 3 nm for the studied system. At temperatures higher than 670 K the dehydration proceeds more rapidly. However, in this temperature range, nanoparticles start re-crystallizing and sintering. Thus, they become larger, while their relative number decreases rapidly with temperature.

A new phenomenon of increase of interlayer distance in MgO crystallites was observed. The interlayer distance increases with decrease of nanoparticle size.

By this work we demonstrate the significance of textural transformations typical for topochemical reactions. The detailed analysis of the results of usual chemical-physical methods shows the possibility of thorough investigation of porous material textural evolution.

Acknowledgment. The authors thank Dr. I. Martyanov (Kansas State University) for FTIR analysis and Dr. V. Zaikovskii (Boreskov Institute of Catalysis) for HREM images. The financial support of the U.S. Army Research office and CRDF (Project RC1-2340-NO-02) is acknowledged with gratitude.

References and Notes

(1) Wanke, S. E.; Fiedorow, R. M. J. *Stud. Surf. Sci. Catal.* **1982**, *39*, 601.
(2) Li, Y.-X.; Klabunde, K. J. *Langmuir* **1991**, *7*, 1388.
(3) Li, Y.-X.; Koper, O. B.; Atteya, M.; Klabunde, K. J. *Chem. Mater.* **1992**, *4*, 323.
(4) Richards, R.; Li, W.; Decker, S.; Davidson, C.; Koper, O.; Zaikovski, V.; Volodin, A.; Rieker, T.; Klabunde, K. J. *J. Am. Chem. Soc.* **2000**, *122*, 4921.
(5) Utamapanya, S.; Klabunde, K. J.; Schlup, J. *Chem. Mater.* **1991**, *3*, 175.
(6) Li, Y.-X.; Schlup, J. R.; Klabunde, K. J. *Langmuir* **1991**, *7*, 1394.
(7) Koper, O. B.; Li, Y.-X.; Klabunde, K. J. *Chem. Mater.* **1993**, *5*, 500.
(8) Hooker, P. D.; Klabunde, K. J. *Environ. Sci. Technol.* **1994**, *28*, 1243.
(9) Li, Y.-X.; Li, H.; Klabunde, K. J. *Environ. Sci. Technol.* **1994**, *28*, 1248.
(10) Mishakov, I. V.; Bedilo, A. F.; Chesnokov, V. V.; Filimonova, S. V.; Martyanov, I. N.; Klabunde, K. J.; Volodin, A. M.; Parmon, V. N. *Chem. Mater.*, submitted.
(11) Fenelonov, V. B.; Mel'gunov, M. S.; Mishakov, I. V.; Richards, R. M.; Chesnokov, V. V.; Volodin, A. M.; Klabunde, K. J. *J. Phys. Chem. B* **2001**, *105*, 3937.
(12) Fenelonov, V. B. *React. Kinet. Catal. Lett.* **1994**, *52*, 367.
(13) Fenelonov, V. B. *Kinet. Catal.* **1994**, *35*, 795.
(14) Karnaukhov, A. P.; Fenelonov, V. B.; Gavrilov, V. Yu. *Pure Appl. Chem.* **1989**, *61*, 1913.
(15) Fenelonov, V. B.; Romannikov, V. N.; Derevyankin, A. Yu. *Microporous Mesoporous Mater.* **1999**, *28*, 57.
(16) Gregg, S. J.; Sing, K. S. W. *Adsorption, Surface Area and Porosimetry*, 2nd ed.; Academic Press: London, 1982.
(17) Gavrilov, V. Yu.; Zagrafskaya, R. V.; Karnaukhov, A. P.; Fenelonov, V. B. *Kinet. Catal.* **1981**, *22*, 452.
(18) Kruk, M.; Antochshuk, V.; Jaroniec, M.; Sayari, A. *J. Phys. Chem. B* **1997**, *103*, 10670.
(19) Jaroniec, M.; Kaneko, K. *Langmuir* **1997**, *13*, 6589.
(20) Pilling, M. B.; Bedworth, R. E. *J. Inst. Met.* **1923**, *1*, 529.